Influence of semi-crystalline microstructure on gas permeability of Poly(Ether-Ketone-Ketone)

Tristan Durand, O. de Almeida

Influence of semi-crystalline microstructure on gas permeability of Poly (Ether-Ketone-Ketone)

T. Durand , O. De Almeida *

Institut Clément Ader, Université de Toulouse, CNRS, UMR 5312, IMT Mines Albi, UPS, INSA, ISAE-SUPAERO, Campus Jarlard, 81013, Albi, France

Keywords:
Gas permeability
Crystallinity
PAEK

In a context of ecological transition, aeronautics is moving towards the development of hydrogen-powered aircraft for which lightweight, long-lasting and tough storage tanks must be developed. Among other properties, the tightness of tanks made of polymer and composite materials is of prime importance. This study thus aims at understanding the permeation phenomena through Poly-Ether-Ketone-Ketone (PEKK), which is one of the thermoplastic polymers considered for tank manufacture. In order to better understand the phenomena governing gas permeability, tests were carried out on different PEKK grades of different T/I ratios and degree of crystallinity. The results show that the crystallinity ratio is not the only factor that governs gas diffusion and solubility, but that permeability also depends on PEKK semi-crystalline microstructure. Even if considering crystallites organization through a tortuosity factor improves permeability predictions, permeability can be better understood using a 3 phases description of PEKK microstructure considering distinct contributions of the rigid and mobile amorphous fractions (RAF and MAF). It appears that the MAF permeation does not depend on PEKK T/I ratio, but that gas diffusion and solubility increase for RAF when increasing T/I ratio, thus counterbalancing the blocking effect of crystallites.

1. Introduction

Against a backdrop of global warming, various sectors of industry and transport are seeking to limit their greenhouse gas emissions. Decades ago, one solution was to reduce the weight of aircrafts by changing the materials used. If we compare the A300 of the 1970s with the A350 of the 2000s, the mass proportion of composites has increased by around 40 % [1]. Today, at the dawn of hydrogen-powered vehicles, this quest for weight savings remains a priority in order to save more energy than before. In the automotive sector, there are already hydrogen-powered cars equipped with “type IV” tanks. This categorization is based on their composition, ranging from type I (made entirely of metal, holding 200 bar) to type IV (carbon fiber composite structure with polymeric liner at 350–700 bar) and soon to type V (all composite without liner at 1000 bar) [2]. The development of hydrogen (H_2) storage tanks made from organic materials is an essential prerequisite for the deployment of these technologies in the transport sector. Whether stored in a gaseous state under pressure, or in a liquid state under cryogenic conditions, reducing tank mass remains essential. The manufacture of storage tanks using high-performance composites reinforced with long fibers thus represents a relevant option. Storing hydrogen with polymeric or composite materials however remains a challenge due to the low steric hindrance of the dihydrogen molecule. Controlling tank leakage therefore requires a perfect understanding of permeation phenomena.

Among the possible matrices of composites, thermoplastics represent an interesting option as they allow the structures to be repaired, welded and recycled [3]. The permeability of a thermoplastic material depends on several parameters, such as its state (glassy or rubbery [4,5]), its molecular weight [6], but above all its crystallinity. Indeed, the crystalline microstructure of semi-crystalline thermoplastic polymers is a key factor of gas solubility and diffusion in thermoplastic matrix polymers and composites [7–9]. Unlike the amorphous phase, crystallites are formed of organized macromolecules, which packing locally increases density. This density makes them impermeable to gases, even in the case of gases composed of small molecules such as dihydrogen or helium.

Semi-crystalline Poly(Aryl-Ether-Ketone) (PAEK) polymers are of particular interest as they are considered promising candidates for the manufacture of large storage tanks. Composites involving these high-performance thermoplastic matrices are already well-established in the aeronautics sector, thanks to their ability to be used in the

manufacture of composite parts using automated processes such as filament winding, Automated Fiber Placement (AFP), etc. [10]. This particular interest in this material compared to other high-performance matrices is mainly due to its high glass transition temperature, which implies excellent thermal stability. In addition, its mechanical and chemical resistance make it the material of choice for the manufacture of tanks [11]. Among the different PAEK polymers, the best-known is Poly (Ether-Ether-Ketone) (PEEK), but Poly(Ether-Ketone-Ketone) (PEKK) is currently regarded for its lower melting point, better mechanical properties, etc. The difference between these two polymers resides mainly in the replacement of an ether function by a ketone function.

The physico-chemical properties of PEEK and PEKK have already been extensively studied [10,12–19]. However, few, if any, focused on the correlation between their crystallinity and the permeation behavior. This study therefore aims to investigate the gas permeation of PAEK polymers, and in order to understand the role of crystalline microstructure, the behavior of three different grades of PEKK that differ in terms of crystallinity and molecular structure was analyzed.

The permeation behavior was investigated with helium, and diffusion and solubility coefficients are correlated with the characteristics of the semi-crystalline microstructure of the three PEKK grades. The data collected for the different grades and different crystallinities are then analyzed using different permeability models adapted to semi-crystalline polymers.

2. Materials and methods

2.1. PEKK samples

Poly-Ether-Ether-Ketone (PEKK) is a synthetized from the copolymerization of two ether-ketone-ketone isomers. Different PEKK grades can thus be obtained depending on the ratio of Terephthaloyl (para) to Isophthaloyl (meta) monomers (Fig. 1).

Changing the T/I ratio affects PEKK's ability to crystallize. Indeed, the more linear T monomers are, the easier it is for the macromolecules to organize into crystallites.

In this study, 3 PEKK grades of different T/I ratios are investigated. They were supplied by ARKEMA in the form of 100 µm films, and referred as 6002, 7002 and 8002 grades for 60, 70 and 80%mol. of Terephthaloyl monomers respectively. Table 1 shows the physico-chemical properties of the 3 PEKK grades. As previously mentioned, due to chain mobility, an increase in melting and glass transition temperature can be observed with the increase in the T/I ratio.

As film extrusion induces high cooling rates, the as-received films have a very low crystallinity. However, achieving a heat treatment at the rubbery state (from 200 °C to 240 °C depending on the T/I ratio) enabled their crystallinity to be increased by cold crystallization (Fig. 2). Two microstructures are thus analyzed in this study for each PEKK grade: the

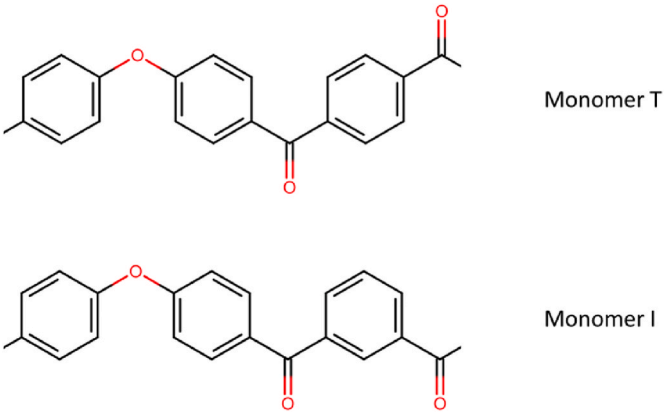

Fig. 1. T and I monomer representation.

Table 1
Thermal and chemical properties of the PEKK grades of different T/I ratios considered in this study.

PEKK	6002	7002	8002
Chemical formula	$[C_{20}H_{12}O_3]_n$		
T_g (°C)	160	162	165
T_m (°C)	305	332	358
T/I Ratio	60/40	70/30	80/20

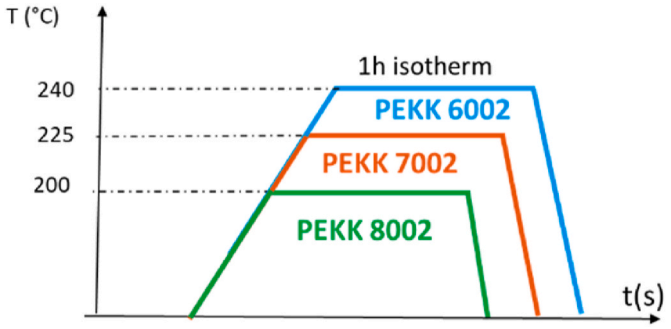

Fig. 2. Schematic of heat treatments applied to PEKKs films according to their T/I ratio.

films as received with low crystallinity (AR) and a cold-crystallized semi-crystalline film resulting from a 1-h heat treatment (CC). This heat treatment resulted in homogeneous and highly crystalline films for each grade. Many heat treatment conditions were tried to prepare films of intermediate crystallinity, but the shrinkage of stretched films occurring during heat treatments, the restricted temperature range between the T_g and T_m of 6002 PEKK grade and the high crystallization kinetics of 7002 and 8002 PEKK grades did not allow satisfactory samples with different crystallinity rates to be obtained with the furnaces available.

2.2. DSC measurements

The mass crystallinity X_c of the initial and treated films was determined by differential scanning calorimetry (DSC PerkinElmer 8000) according to Eq. (5).

$$X_c = \frac{\Delta H_m - \Delta H_{cc}}{\Delta H_{100\%}} \quad \text{(Eq.5)}$$

In Eq. (5), ΔH_m is the melting enthalpy in J.g^{-1}, ΔH_{cc} is the cold crystallization enthalpy and, $\Delta H_{100\ \%}$ is the melting enthalpy of PEKK crystals (assumed equal to 130 J g^{-1} [12]). The measured degree of crystallinity for the as-received (Fig. 3) and heat-treated (Fig. 4) film samples are summarized in Table 2.

Cold crystallization yielded crystallinities ranging from 22 % for 6002 to 33 % for 8002. As expected, the degrees of crystallinity of cold crystallized samples vary according to the T/I ratio, due to the increasing proportion of linear monomers.

2.3. XRD measurements

X-ray diffraction (XRD) analysis was carried out using a Malvern PANalytical Empyrean Series 3 X-ray diffractomer. This instrument has been used in Wide-Angle X-ray Scattering (WAXS) mode and Small-Angle X-ray Scattering (SAXS) configurations. For both techniques, the samples studied were 25 mm diameter disks taken from 100 µm thick films.

WAXS allows crystallite width L_c to be measured using Scherrer's equation (Eq. (6).

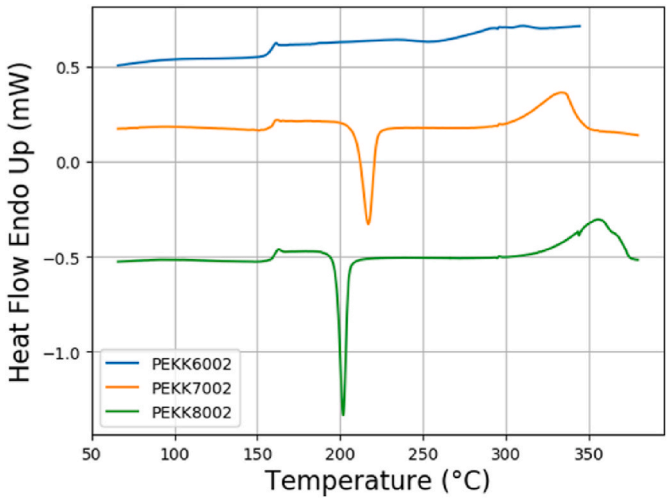

Fig. 3. DSC thermograms of as-received amorphous PEKK films (heating rate of 10 °C.min^{-1}).

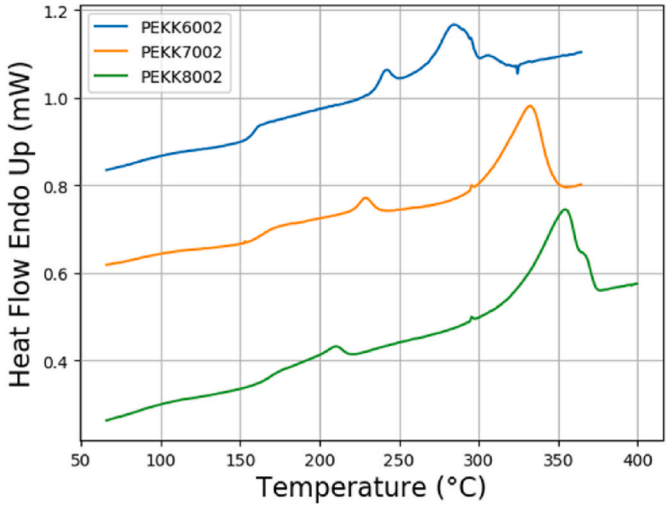

Fig. 4. DSC thermograms of cold-crystallized PEKK films (heating rate of 10 °C.min^{-1}).

Table 2
Degree of crystallinity X_C of PEKK samples determined by DSC (AR: As-Received; CC: Cold-Crystallized).

PEKK sample	6002		7002		8002	
	AR	CC	AR	CC	AR	CC
X_c (%)	1.1	22.0	2.6	28.0	6.2	33.0

$$L_{c,hkl} = \frac{0,9 \times \lambda_{Cu}}{FWHM \times \cos(\theta_{hkl})} \quad \text{(Eq.6)}$$

In Eq. (6), $\lambda_{Cu} = 0.154\,nm$ is the wavelength of the K_α copper x-rays source, θ is Bragg's angle in radians and FWHM is the half-height width of diffraction peaks of 2θ angle in radians.

SAXS mode was used to determine the average thickness W_c of crystalline lamella and the crystal/amorphous long period L_p. To do so, the Mylar sample holder was first subtracted from the raw SAXS signal of PEEK measurement [22]. The resulting signal is a quantity of photon scattered towards a θ angle direction from the incident beam. This angle was converted into the scattering vector q:

$$q = \frac{4\pi}{\lambda_{Cu}} \sin(\theta) \quad \text{(Eq.7)}$$

This subtracted signal was then smoothed by a Savitzky-Golay method and the Fourier transformation γ(r) of the resulting signal ([23,24]) was achieved using Eq. (8).

$$\frac{\gamma(r)}{\gamma_0} = \frac{\int_0^\infty q^2 I(q)\cos(qr)dq}{\int_0^\infty q^2 I(q)dq} \quad \text{(Eq.8)}$$

The curve obtained from this transformation (Fig. 5) could finally be used to determine the crystal/amorphous long period L_p and the thickness of the crystalline lamellae W_c [23].

2.4. Gas permeability measurements

Permeability was measured using a homemade test device specially developed for the purpose of the HYPOCCRYT project (Hydrogen Permeability of Organic Composites at Cryogenic Temperatures). It is based on the principle of partial pressure difference between an upstream chamber connected to the gas inlet and a detection chamber equipped with gas sensors (Fig. 6). The gas passing through the material can be detected either by a cold cathode pressure sensor in a test configuration of closed volume, i.e. where gas permeation leads to a pressure balance between the two chambers, or by a mass spectrometer when using a constant gas inlet pressure and continuously vacuuming the detection chamber. In this study, all permeability measurements were achieved using this second configuration. The pressure was set at 0.5 bar in the inlet chamber and p < 10^{-4} mbar in the detection chamber. Gas permeability was characterized using helium 6.0, which is close in size to hydrogen [25] and the polymer samples had a thickness of 100 μm and a diameter of about 60 mm.

Experimentally, permeability, diffusion and solubility can be determined from the quantity of gas passing through the sample over time.

Here, given the use of a mass spectrometer, the change in helium partial pressure with time in the detection chamber was used to determine permeability parameters (red dots in Fig. 7). The permeability coefficient was obtained with Eq. (9) from the steady-state helium partial pressure and parameters such as chamber volume, pump flow rate, etc.

$$P = \frac{p_{ST}\dot{V}}{R\,T} \times \frac{th}{A\,\Delta p} \quad \text{(Eq.9)}$$

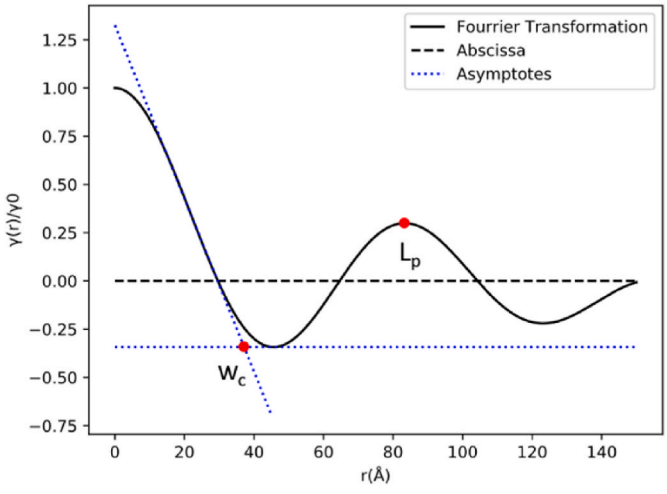

Fig. 5. Fourier transform representation of SAXS signal.

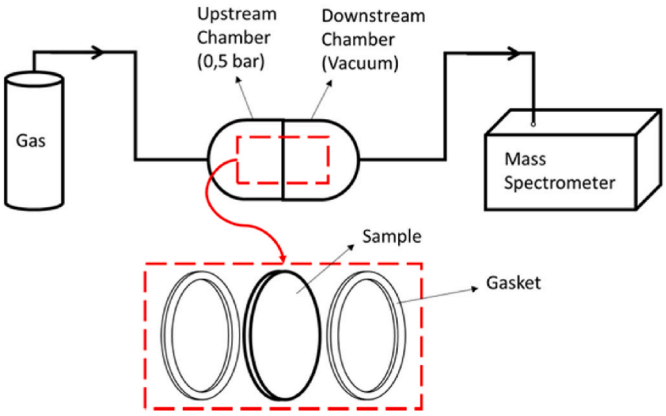

Fig. 6. Schematic of gas permeability device.

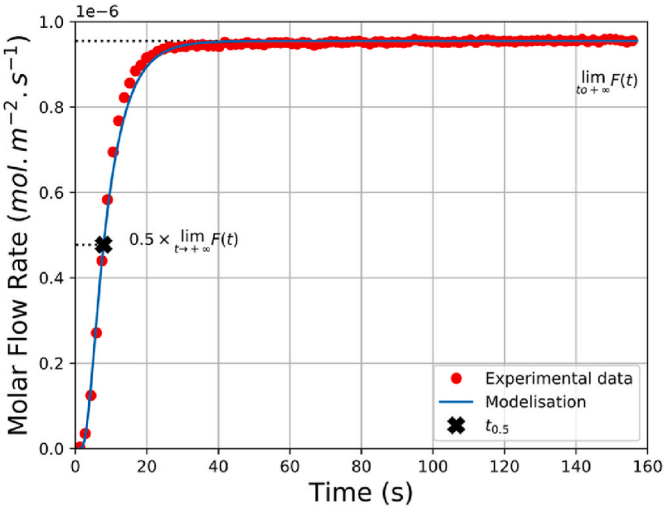

Fig. 7. Experimental permeation flow rate measurement recorded over time on amorphous PEKK 6002 film and model prediction assuming a Fickian diffusion and Henry's law of solubility (Eq. (12)).

In Eq (9), p_{ST} corresponds to the partial pressure of helium at the steady state (Pa), $\dot{V}$ is the volume flow rate of the turbomolecular pump ($m^3.s^{-1}$), A is the sample permeated surface (m), Δp is pressure difference between the inlet and detection chambers, R is the gas constant (8.314 J mol^{-1} K^{-1}) and T and th refer to the sample temperature (K) and thickness respectively. Permeability P of n_{gas} gas moles per unit of time dt and pressure dp is then expressed in the following units:

$$P = \frac{n_{gas}[mol] \times th[m]}{dt\,[s] \times dp[MPa] \times A[m^2]} \quad \text{(Eq.4)}$$

In the case of a Fickian diffusion process, the diffusion coefficient is classically determined by the time-lag θ, i.e. the transition time to steady state. However, the time to reach half of the steady-state partial pressure $t_{0.5}$ was here preferred for its robustness (Fig. 7). This was possible thanks to the use of a constant inlet pressure configuration [26]. Indeed, the diffusion coefficient D is then simply given by Eq. (10) and it can be simply determined from $t_{0.5}$ and the sample thickness th.

$$D = \frac{th^2}{7.199 t_{0.5}} \quad \text{(Eq.10)}$$

Finally, with P expressed as $D \times S$, solubility could be obtained from the ratio of permeability to diffusion (Eq. (11)).

$$S = \frac{P}{D} \quad \text{(Eq.11)}$$

In order to confirm the validity of the permeation definition, and in particular the validity of the Fickian diffusion and Henry's solubility in PEKK polymers, the analytical solution of the permeation problem was computed with the identified P and D parameters [20,26]. The instantaneous molar flow rate F in $mol.m^{-2}.s^{-1}$ was computed using Eq. (12) and the resulting model prediction is plotted along with experimental data in Fig. 7.

$$F(t) = P\Delta p\left(\frac{4}{\pi^2 Dt}\right)^{\frac{1}{2}} \sum_{n=1,3,5,\ldots}^{\infty} e^{-\frac{n^2 th^2}{4Dt}} \quad \text{(Eq.12)}$$

The analytical solution well predicts the experimental permeation flow rate over the entire permeation test. This confirms that the identified diffusion and permeability coefficients are representative of material's behavior because the Fickian diffusion description applies to PEKK as well as Henry's law of solubility. This was actually expected since previous literature on PEEK permeation already reported the pertinence of coupling Fickian diffusion with Henry sorption for this class of polymers [27] with helium, a low condensable gas.

3. Experimental permeability, diffusion and solubility

Helium permeability, diffusion and solubility results for amorphous and semi-crystalline PEKK polymers are summarized in Table 3 and plotted as a function of the corresponding degree of crystallinity (Fig. 8, Fig. 10).

The results displayed in the figures are the average of experimental data obtained from two different samples for most conditions and from two repeated measurement on each sample. The error bars displayed in Fig. 8 for permeability take into account the samples variability, the uncertainty of mass spectrometer measurement, films thickness variability, uncertainty of the samples permeated surface, and the uncertainty of gas inlet pressure. For diffusion (Fig. 9), thickness measurement variability and uncertainty of time-lag assessment on the transient phase were taken into account to define the error bars. Finally, the error bars for solubility (Fig. 10) result from permeation and diffusion errors.

Preliminary analysis of the results confirms the blocking effect of the crystalline phase on gas permeability. In fact, two populations are visible: amorphous polymers have a permeability around 1.8 times greater than crystalline polymers. Nevertheless, the results in Fig. 8 also show that, contrary to what might be expected from literature [27], gas permeation does not necessarily decreases with crystallinity. Indeed, the 3 heat-treated grades have very different crystallinity rates but very similar permeabilities. This indicates that the T/I ratio has an impact on permeability and that the 3 materials should be considered separately. The influence of the T/I ratio is confirmed by distinguishing the contributions of D and S to permeability (Figs. 9 and 10). While solubility remains constant for all 3 materials as a function of crystallinity, the evolution of diffusion with crystallinity varies with the T/I ratio.

Table 3
Experimental permeability ($mol.m^{-1}.s^{-1}.MPa^{-1}$), diffusion ($m^2.s^{-1}$) and solubility ($mol.m^{-3}.MPa^{-1}$) coefficients of as-received (AR) and cold-crystallized (CC) PEKK grades of different T/I ratios.

PEKK		X_c	P x 10^9	D x 10^{10}	S
6002	AR	1.10	1.90	1.69	11.3
	CC	22.0	0.978	1.38	7.07
7002	AR	3.60	1.91	1.71	11.3
	CC	28.0	0.958	1.39	6.89
8002	AR	6.20	1.82	1.70	10.7
	CC	33.0	0.998	1.44	6.91

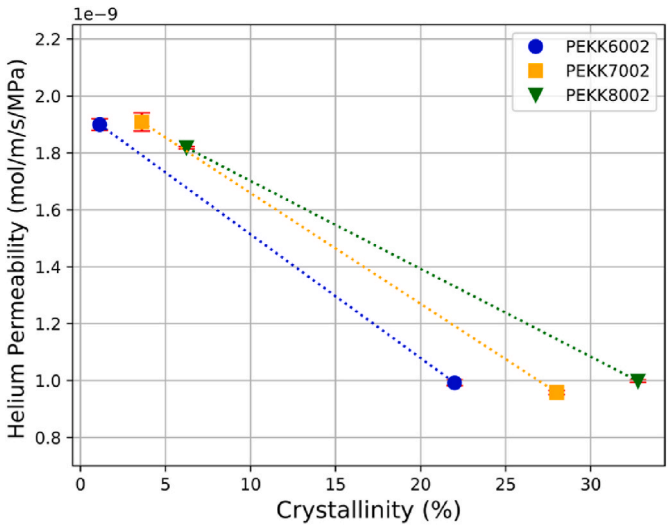

Fig. 8. Evolution of PEKK permeability as a function of crystallinity for different T/I ratios.

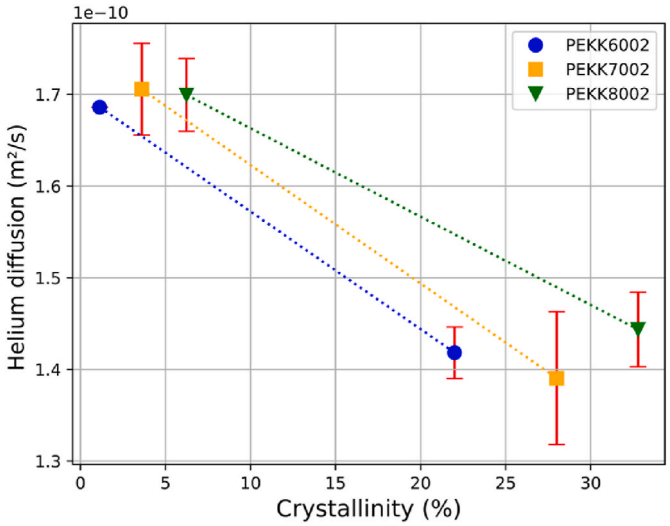

Fig. 9. Evolution of PEKK diffusion as a function of crystallinity for different T/I ratios.

4. Two-phase semi-crystalline model

The first hypothesis that can be put forward to explain the difference in behavior of the 3 PEKK grades is that their amorphous phase exhibits different behaviors as a function of the T/I ratio (the crystalline phase being assumed to be impermeable). This can be analyzed by identifying the properties of the amorphous phase of each grade, considering a two-phase crystal/amorphous microstructure (Eq. (13)) [9] and distinct diffusion D_a and solubility S_a coefficients for each amorphous fraction X_a of the PEKK grades.

$$X_c + X_a = 1 \qquad \text{(Eq.13)}$$

This approach consists in describing the permeability P_{SC} of each semi-crystalline PEKK grade using a distinct amorphous phase permeability P_a for each PEKK grade according to Eq. (14).

$$\begin{aligned} P_{SC} &= D_{sc} \times S_{sc} \\ &= (1 - X_c) D_a \times (1 - X_c) S_a \\ &= (1 - X_c)^2 P_a \end{aligned} \qquad \text{(Eq.14)}$$

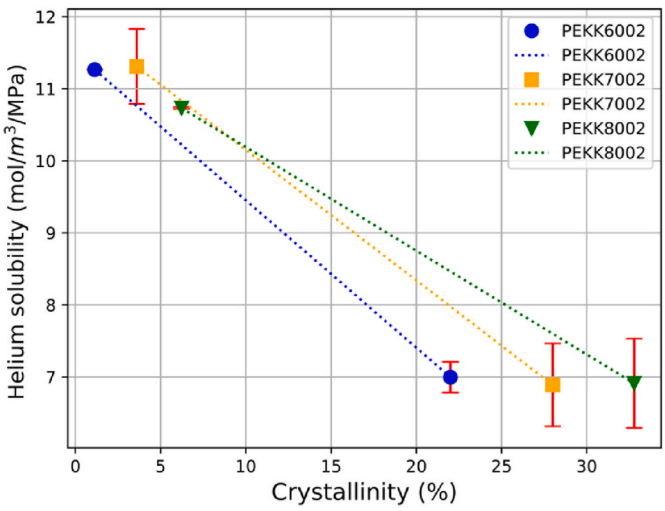

Fig. 10. Evolution of PEKK solubility as a function of crystallinity for different T/I ratios.

The prediction of permeability as a function of crystallinity is globally described by the two-phase model (Fig. 11), since crystallinity remains the main factor in the decrease in permeation. A relative mean error of 6 % is obtained for the two-phase model (8.7 % for the 6002, 5.3 % for the 7002 and 3.7 % for the 8002). The theoretical permeabilities of the amorphous phase of 6002, 7002 and 8002 grades estimated by this model are 1.79×10^{-9}, 1.95×10^{-9} and 2.14×10^{-9} mol/m/s/MPa respectively. However, the model considers a linear dependence of diffusion and solubility to the degree of crystallinity, and it finally lacks in predicting the constant permeability observed for the CC grades of different T/I ratios. Indeed, according to Eq. (14), whatever the grade, P_{SC} tends to zero when increasing crystallinity. Hence, the higher the crystallinity, the lower is the influence of the amorphous phase on polymer permeability.

5. Two-phase model with tortuosity

In the context of a two-phase description of semi-crystalline polymers, permeability prediction can be improved by considering the microstructural organization of the amorphous and crystalline phases in

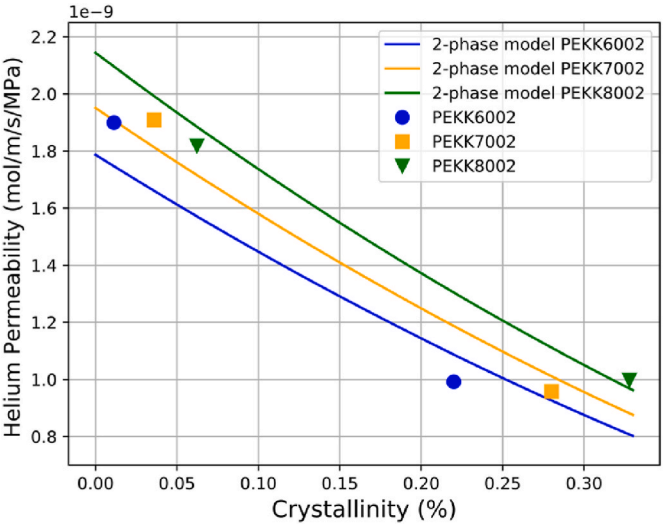

Fig. 11. Permeability prediction from the two-phase model by inverse method, and values of diffusion coefficients D_a and solubility S_a of the amorphous phase identified from the two-phase model (Eq. (14)).

the permeation definition. To do so, microstructure parameters were introduced in gas diffusion definition according to Eq. (15). This approach, that was already reported in literature [28], consist in taking into account the tortuosity of the diffusion path by means of a dimensionless tortuosity factor τ and the mobility of the amorphous phase using a dimensionless chain immobilization factor β. This latter represents the effect of crystallites or cross-linking networks on chain mobility [10,29].

In this approach of permeation process, solubility is assumed occurring solely in the amorphous phase. Its expression thus remains unchanged [29], which yields Eq. (16) for permeability.

$$D_{sc} = \frac{D_a}{\tau\beta} \quad \text{(Eq.15)}$$

$$P_{SC} = \frac{1 - X_c}{\tau\beta} P_a \quad \text{(Eq.16)}$$

According to Ref. [30], tortuosity τ represents the additional path the gas must complete to circumvent impermeable obstacles in the material, as shown in Fig. 12.

These impermeable obstacles can be fibers or fillers, but also polymer crystallites according to Ref. [28]. In the case of a semi-crystalline polymer, tortuosity can be expressed as:

$$\tau = 1 + \frac{\frac{L_c}{2}}{W_c} X_c \quad \text{(Eq.17)}$$

in which L_C and W_C are respectively the width and thickness of crystallites. However, this formula only considers obstacles that are parallel to each other, and a correction coefficient taking into account the orientation angle θ of crystallites must be added in the definition of tortuosity [31]:

$$\tau = 1 + \left[\frac{L_c}{2W_c} X_c \times \cos(\theta)^2\right] \quad \text{(Eq.18)}$$

Considering $G = (1/2) \times \left(3\cos(\theta)^2 - 1\right)$, the expression for permeability yields:

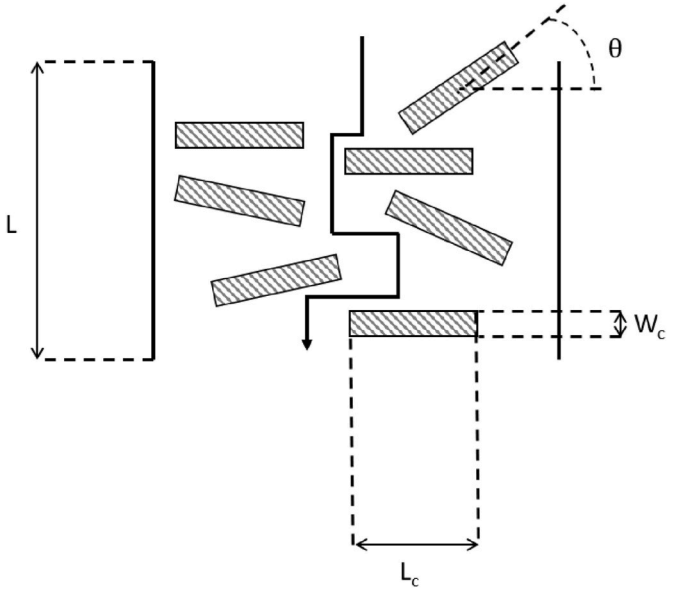

Fig. 12. Schematic of tortuosity principle within a semi-crystalline polymer material containing crystallites of width L_C, thickness W_C and orientation θ (adapted from Ref. [31]).

$$P_{SC} = \frac{(1 - X_c)P_a}{\left[1 + \left[\frac{L_c}{2W_c} X_c \times \frac{2}{3}\left(G + \frac{1}{2}\right)\right]\right]\beta} \quad \text{(Eq.19)}$$

Since the orientation of crystallites within a semi-crystalline microstructure is difficult to determine, the extreme cases of perfectly oriented crystallites ($G = 1$), randomly oriented crystallites ($G = 0$) and oriented orthogonal to the film plane ($G = -1/2$) were considered.

Regarding the immobilization factor β, Kanesugi et al. demonstrated that the value of β is very close to 1 for gases with low condensability, such as helium or dihydrogen [28,29]. This factor was thus considered equal to unity in this study.

In order to explore the accuracy of Eq. (19) to predict the gas permeability of PEKK grades, the dimensions of the crystalline structure were assessed using SAXS and WAXS data. The average size of crystallites L_C and W_C were determined for the three semi-crystalline samples (Table 4). It appears that the dimensions of crystallite are relatively close from one PEKK to another, but a slight increase in crystallite width and thickness can be observed as the T/I ratio increases.

Though, it must be noted that the WAXS scans show evidence of the formation of two crystal types in the three heat-treated PEKK grades: the type I crystals, that are characterized by the diffraction peaks of $(110)^I$, $(200)^I$ and $(211)^I$ planes, and the type II crystals which presence is demonstrated by the diffraction peak related to the $(020)^{II}$ plane [16]. This latter is specific to PEKK [16], and is most likely formed during cold-crystallization [16]. The distinction of the diffraction peaks related to each crystal form indicates that the average size of Form I and Form II crystals are different. In 6002, 7002 and 8002 grades, L_C crystal lengths are 9.85 nm, 12.33 nm and 12.5 nm for form I respectively, and 20.25 nm, 25.42 nm and 16.06 nm for form II respectively. Nevertheless, whatever the type of crystal, the impermeability of the crystalline structure to gases remains a reasonable assumption, and the two forms were therefore assumed to be equivalent. Moreover, according to diffraction peak areas the proportion of form II crystals is negligible as regards to form I and an equivalent single crystal form was therefore considered from both types of crystal, although they may affect the behavior of the surrounding amorphous phase differently.

The application of the tortuosity model (Eq. (19)) with crystallite dimensions in Table 4 yields the results shown in Table 5. As the permeability value of 100 % amorphous polymers is not known (as-received films have a slight crystallinity and are not fully amorphous), equation (Eq. 19) was used to calculate it based on the experimental data on cold-crystallized samples (P_{CC}). The permeability values obtained for the fully amorphous polymers P_a are significantly lower than those obtained for the as-received samples P_{AR} as characterized by the relative difference between the two values ε. The model taking into account crystallites oriented perpendicular to the gas flow (G = 1, planar) is the one giving the lowest ε value, and therefore this configuration is the one offering the best prediction of permeation behavior using the current tortuosity model.

Nevertheless, these results must be nuanced since the actual complexity of the crystalline microstructure is only considered by means of three parameters in Eq. (19). Differences between PEKK grades that are noticeable on WAXS scans in Fig. 13 are thus simplified and the consequence on tortuosity can hardly be assessed. Indeed, the relative peak heights on the WAXS scans provide indications about films' orientation, and in the case of PEKK grades, the heights of the diffraction peak of $(110)^I$ plane reveal some differences. A sharp peak is clearly

Table 4
Crystallites' thicknesses W_C and widths L_C in cold-crystallized PEKK grades determined from WAXS/SAXS experiments (Figs. 5 and 13).

	6002	7002	8002
L_C **(nm)**	12.43	12.72	13.12
W_C **(nm)**	3.666	3.718	3.738

Table 5
Permeability prediction [mol.m^{-1}.s^{-1}.MPa^{-1}] considering tortuosity induced by crystallites in the three PEKK grades of different T/I ratios, when assuming stacks of parallel crystallites (oriented) and assuming randomly oriented crystallites (Random). P_{CC} and P_{AR} correspond to the permeability of cold-crystallized (AR) and as-received (AR) film samples respectively.

		6002	7002	8002
Exp.	P_{CC} x 10^9	0.995	0.968	1.00
	P_{AR} x 10^9	1.90	1.91	1.82
Unoriented (G = 0)	P_a x 10^9	1.10	1.11	1.19
	ε (%)	42.1	41.9	34.6
Oriented Planar (G = 1)	P_a x 10^9	1.35	1.42	1.58
	ε (%)	28.9	25.7	13.2
Oriented Orthogonal (G = −1/2)	P_a x 10^9	0.98	0.961	1.00
	ε (%)	48.4	49.7	45.1

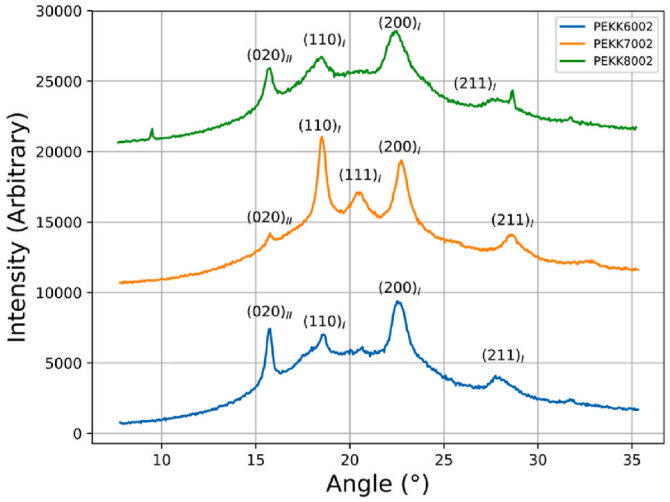

Fig. 13. XRD WAXS scans of PEKK 6002, 7002 and 8002 with annotation of plane orientations and crystallographic shapes.

visible for grade 7002 while it is hardly visible for the two other materials. Also, the relative height of peaks $(110)^I$ to $(200)^I$ varies according to PEKK grade, which is most likely due to the use of a different film extrusion process for manufacturing grade 7002 film compared to PEKK grades 6002 and 8002. Yet, surprisingly, the planar configuration (G = 1) remains the most accurate configuration for predicting permeability for all PEKK grades. Therefore, although tortuosity remains a valid approach, Eq. (19) does not sufficiently describe the actual microstructure of polymers induced by the initial film extrusion processing and the following heat-treatment. The size distribution of crystalline entities or their type and organization within spherulites are summarized into the only three parameters τ, β, and θ and this approach then necessarily lacks in providing a general understanding of the relation between the semi-crystalline microstructure and gas permeability. Refining the description of PAEK crystal entities would allow adding a higher number of parameters into the tortuosity model, which in the end would provide a better prediction of the gas path and hence gas permeabilities within PEKK grades. The three-dimensional morphology of PEKK crystals is, however, difficult to characterize and modifications of tortuosity definition then would require numerical inverse analysis. Instead of focusing on the crystallites themselves, the overall description of the semi-crystalline microstructure was thus reconsidered.

6. Three-phase semi-crystalline model

In order to better describe the microstructure organization, various isothermal and non-isothermal crystallization conditions were applied during DSC experiments. The melting enthalpy and the heat flow step at the glass transition temperature T_g were recorded. Doing so, various couples of degrees of crystallinity and specific heat change at T_g were obtained from totally amorphous up to about 30 % crystallinity.

Surprisingly, DSC results revealed a non-linear relationship between the material's enthalpy of fusion and the corresponding change of heat capacity at T_g (Fig. 14). Also, all data from the three materials superimpose well on a chart $\Delta H_m = f(\Delta C_p)$ and a unique trend can be defined that applies to all PEKK grades whatever their crystallinity.

This non-linearity indicates that the semi-crystalline microstructure is not simply composed of two independent amorphous and crystalline phases, but that the crystal/amorphous organization must be reconsidered. This interaction between the crystalline and amorphous phases has already been reported in literature, and many authors actually agree on the existence of a specific amorphous phase known as Rigid Amorphous Fraction" (RAF) located around the crystals (Fig. 15) [17–19,32,33]. This was demonstrated using DMA experiments, through the analysis of secondary relaxations, and more particularly the α-relaxation that is assumed correlated to the presence of a RAF in semi-crystalline polymers. The introduction of this 3-phases description has already been used in many fields and in particular for explaining polymer mechanical behavior [17].

This distinction within the amorphous phase of a Mobile Amorphous Fraction (MAF), which behavior is not influenced by the crystalline phase, and of a Rigid Amorphous Fraction (RAF), which mobility is constrained by the involvement of chains in crystals [34,35], allows assuming different solubility and diffusions coefficients for each fraction.

Considering both RAF and MAF contributions, the equilibrium equation for the semi-crystalline polymeric system can be defined with Eq. (20).

$$RAF + MAF + X_c = 1 \qquad \text{(Eq.20)}$$

The mass proportions of mobile and rigid amorphous phases are estimated assuming that the heat flow step on the DSC scans at the glass transition temperature $\Delta C_p(T_g)$ (in J.g^{-1}.K^{-1}) is only related to the change in mobility within the mobile amorphous phase. The MAF was then determined using Eq. (21) in which $\Delta C_p^{0\%}(T_g)$ is the change in thermal capacity at the glass transition temperature for a 100 % amorphous polymer in J.g^{-1}.K^{-1}.

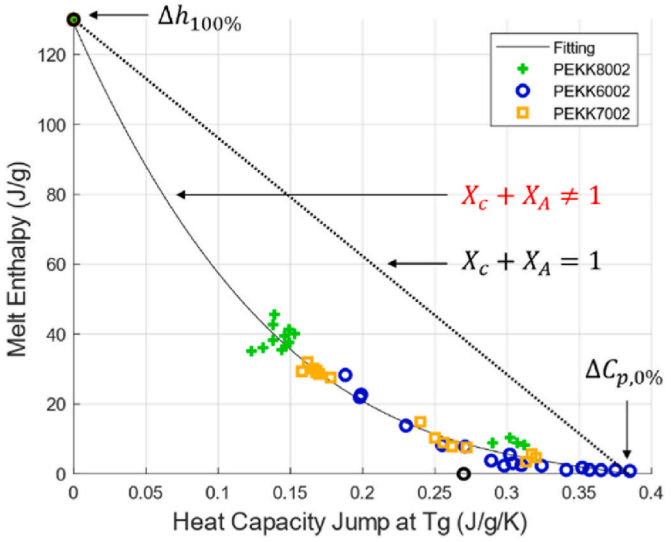

Fig. 14. Evolution of the melting enthalpy of a semi-crystalline polymer ($\Delta H_m - \Delta H_{cc}$) as a function of the corresponding change in heat capacity at T_g (the black mark indicates the value of $\Delta C_p^{0\%}$ given in Ref. [34] for PEEK).

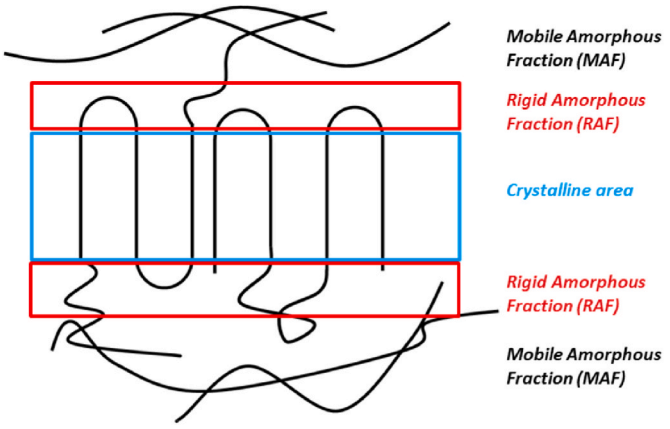

Fig. 15. Schematic representation of a crystalline lamella (blue), a rigid amorphous phase (red) and a mobile amorphous phase (black). (For interpretation of the references to colour in this figure legend, the reader is referred to the Web version of this article.)

$$MAF = \frac{\Delta C_p(T_g)}{\Delta C_p^{0\%}(T_g)} \quad \text{(Eq.21)}$$

The value used for $\Delta C_p^{0\%}(T_g)$ is simply obtained from the extrapolation of experimental data in Fig. 13 starting from the enthalpy of fusion of a PEKK crystal $\Delta H_m^{100\%} = 130$ J.g^{-1}. A polynomial fit led to a value of 0.384 J g^{-1} K^{-1}, and it should be noted that it differs from that of PEEK available in the literature (0.27 J g^{-1} K^{-1} given in Refs. [35–38]).

The mass fractions of the 3 phases calculated using Eq. (20) and Eq. (21) for each PEKK are summarized in Table 6. Based on the three-phase description of the semi-crystalline microstructure of the various PEKK grades, it was then possible to express polymers permeability from the contribution of RAF and MAF [26] with Eq. (22)–(24).

$$D_{X_c} = MAF\, D_{MAF} + RAF\, D_{RAF} \quad \text{(Eq.22)}$$

$$S_{X_c} = MAF\, S_{MAF} + RAF\, S_{RAF} \quad \text{(Eq.23)}$$

$$P_{X_c} = D_{X_c} \times S_{X_c} \quad \text{(Eq.24)}$$

P_{Xc}, D_{Xc}, S_{Xc} respectively correspond to permeability, diffusion and solubility of the semi-crystalline polymers with a degree of crystallinity X_C. Based on MAF and RAF (**Table 6**), this model allows to decouple their respective contributions to diffusion and solubility. Two values are therefore to be determined for diffusion (D_{MAF} and D_{RAF}) and solubility (S_{MAF} and S_{RAF}) from two equations per system (Eq.25 and Eq.26).

$$\begin{bmatrix} D_{MAF} \\ D_{RAF} \end{bmatrix} = \begin{bmatrix} MAF_{CC} & RAF_{CC} \\ MAF_{AR} & RAF_{AR} \end{bmatrix}^{-1} \begin{bmatrix} D_{CC} \\ D_{AR} \end{bmatrix} \quad \text{(Eq.25)}$$

Table 6
Crystalline mass fraction (X_c), Mobile Amorphous Fraction (MAF) and Rigid Amorphous Fraction (RAF) for as-received (AR) and cold-crystallized (CC) PEKK grades.

PEKK		X_c (%)	MAF (%)	RAF (%)
6002	AR	1.10	90.3	8.60
	CC	22.0	47.0	31.0
7002	AR	3.60	81.2	15.2
	CC	28.0	40.0	32.0
8002	AR	6.20	75.4	18.4
	CC	33.0	30.0	37.0

$$\begin{bmatrix} S_{MAF} \\ S_{RAF} \end{bmatrix} = \begin{bmatrix} MAF_{CC} & RAF_{CC} \\ MAF_{AR} & RAF_{AR} \end{bmatrix}^{-1} \begin{bmatrix} S_{CC} \\ S_{AR} \end{bmatrix} \quad \text{(Eq.26)}$$

The Diffusion and Solubility coefficients determined for both MAF and RAF of each PEKK grade are displayed in Figs. 16 and 17.

A first analysis of these results (Figs. 16 and 17) shows that diffusion and solubility in the mobile amorphous phase (MAF) are almost identical from one PEKK grade to another. Moreover, the results show that diffusion and solubility coefficients in RAF increase continuously as the T/I ratio increases. This general trend therefore supports the validity of the triphasic approach to describe PEKK permeation.

First considering all grades together, it clearly appears that, overall, gas diffuses better in the RAF than in the MAF and solubilizes better in the MAF than in the RAF. Since RAF is related to the amount of crystals, the higher PEKK crystallinity, the greater is the effect of RAF on permeability. Hence, with increasing PEKK crystallinity, the impermeability of the crystalline phase is counterbalanced by the higher diffusion in the RAF than in the mobile amorphous phase.

Then considering the T/I ratio, the model indicates that diffusion and solubility in the rigid amorphous phase increases with the proportion of Terephtaloyl monomer in PEKK. Therefore, the fact that a constant permeability was observed for the three cold-crystallized films despite different degrees of crystallinity (Fig. 8), can be attributed to the higher diffusion and solubility in the RAF that degrade the impermeability of crystallites.

7. Discussion

Since crystals are assumed impermeable to gas and fully amorphous PEKK materials are considered homogeneous and of same permeability whatever the grade, the biphasic semi-crystalline models, whether tortuosity is considered or not, lacks in predicting the constant permeability observed for the CC grades of different T/I ratios. The distinction within the amorphous phase of two distinct fractions then appears to be the most appropriate approach for describing the particular permeation behavior of PEKK grades. The distinction of two different behaviors for the mobile and rigid amorphous phases allows balancing the impermeability of crystals with a permeable amorphous fraction. This way, different influences of PEKK's degree of crystallinity on permeability can be defined, while maintaining consistency between polymers in the fully amorphous state. The ability of chemical species to permeate through a polymeric matrix is directly correlated to the fraction of free volume. The free volume is the space not occupied by macromolecules in the total volume of the polymer [39]. The free volume f can be defined with

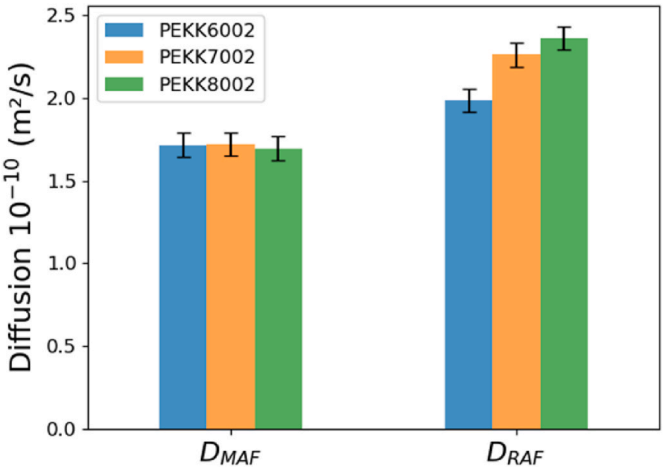

Fig. 16. Diffusion coefficients of the mobile and rigid amorphous phases identified from the three-phase model (Eq. (22)–(24)).

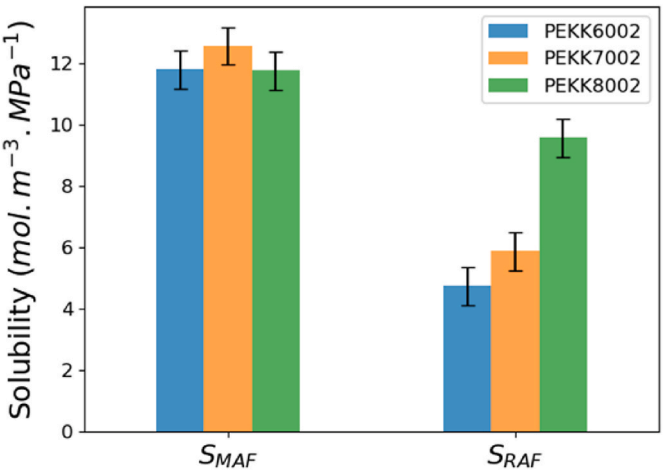

Fig. 17. Solubility coefficients and of the mobile and rigid amorphous phases identified from the three-phase model (Eq. (22)–(24)).

Eq.27 in which V_T is the total volume of the polymer and V_{VDW} corresponds to the theoretical van der Waals volume, i.e. the intrinsic volume of PEKK macromolecules.

$$f = \frac{V_T - V_{VDW}}{V_T} \quad \text{(Eq.27)}$$

Several models of diffusion and solubility as a function of free volume have been proposed, among which the following form is adapted to semi-crystalline polymers [9]:

$$D_a = Ae^{\left(\frac{-B}{f_a}\right)} \quad \text{(Eq.28)}$$

$$S_a = Cf_a \quad \text{(Eq.29)}$$

In Eq.28 & Eq.29, A, B and C are constants associated with the system and f_a represents the fraction of free volume in the amorphous phase. These equations describe that an increase in free volume implies an increase in the coefficient of diffusion, solubility and hence permeability.

Within a polymer, the free volume varies depending on monomer type, thermal history, and physical state. But the consideration of two amorphous fractions also suggests that the free volume, and hence permeability, is also heterogeneous within the amorphous phase. A locally different density and mobility of the polymer chains in the RAF is indeed plausible considering that macromolecules in RAF are partly involved into the formation of crystals. In PEKK grades, according to Eq. (28), the diffusion coefficients D_{RAF} and D_{MAF} (Fig. 16) comply with a larger fraction of free volume in the RAF, i.e. close to crystallites. This is consistent with the conclusions raised by Marano et al. in their study of Poly(Lactic) Acid [40], who concluded that the existence of RAF induces an excess of free volume in the matrix and therefore an increase in gas permeability. For the same material, Guinault et al. [41] also attributed the higher diffusion coefficient to the larger free volume in the RAF.

The presence of the aromatic meta configuration of Isophthaloyl monomer in the structure of PEKK macromolecules (Fig. 1) also supports the assumption of a larger free volume in RAF. Indeed, during PEKK crystallization, the formation of perfect crystals cannot involve meta configurations of PEKK copolymers, as they represent chain irregularities. The chain lengths resulting from the polymerization of isophtaloyl monomer are thus excluded from the crystals, and as a consequence, the concentration of meta configurations might be higher close to crystallites in comparison with the mobile amorphous phase. The rotation of the aromatic group of isophthaloyl group being restricted, the possibility for the macromolecules to organize into a dense structure is restrained, then inducing a larger free volume in the RAF than in the MAF.

Regarding solubility, the distinct contributions of the MAF and RAF on gas barrier properties remains clear according to PEKK results, but the solubility coefficients S_{RAF} and S_{MAF} contradict the conclusion of a larger free volume in RAF. Indeed, according to Eq. (29), the higher S_{MAF} implies a higher free volume in the mobile amorphous phase, while diffusion results indicate the opposite. The reason of such discrepancy is probably due to the use of helium for analyzing PEKK permeability. Helium is a neutral gas with low condensability, and its interaction with macromolecules is thus much lower than in the case of other gases such as carbon dioxide or vapors.

The fact Henry's law perfectly applies to PEKK grades (Fig. 7) actually confirms the absence of interaction of this permeating gas with the polymer. A "Dual-Mode" sorption (Eq. (30)) is generally used for defining the permeability of glassy polymers such as PEKK [9]. Compared to Henry's law, the Dual-Mode involves a Langmuir interaction term accounting for the interaction of the gas with free sites. This term involves a parameter C'_H related to the saturation concentration of free sites and a coefficient b representing the affinity of gas for free volume, porosity, voids, etc.

$$C_{DualMode} = k_D p + \frac{C'_H bp}{1 + bp} \quad \text{(Eq.30)}$$

For helium, it has been demonstrated experimentally on Polymers of Intrinsic Microporosity (PIM), that the parameter b is very low, between 0.1 and 0.4 MPa^{-1} [42,43]. Therefore, since $\lim_{b\to 0} C_{DualMode} = k_D p$, Henry-type sorption behavior applies with helium. Due to the weak interaction of helium with polymers, very low helium solubility coefficients have been reported in the literature [44–46]. Michaels et al. even concluded from their experimental data that the solubility of helium was "abnormal" [47].

Because of low helium solubility and affinity with free sites, permeability is mainly controlled by diffusion [21]. The lower solubility in the RAF of PEKK grades compared to MAF (Fig. 17) then may be the consequence of a dominant diffusion regime over solubility. Indeed, the rapid transport of gas in a diffusion regime can limit the saturation of free volume, and hence solubility, despite the larger free volume in the RAF (Fig. 18).

The differences in RAF behavior between the three PEKK grades (Fig. 16) also indicate that the free volume not only depends on the mobile and rigid amorphous phases but also on the T/I ratio. Here also, this can be correlated to the concentration of meta configurations in the RAF. Indeed, for the same degree of crystallinity, the concentration of meta configurations in RAF might be significantly higher for PEKK 6002 than PEKK 8002. The free volume in RAF then must increase with the T/I ratio, leading to differences in diffusion coefficients. However, the fact the mobile amorphous phase exhibits constant diffusion and solubility whatever the grade suggest that a concentration threshold of meta

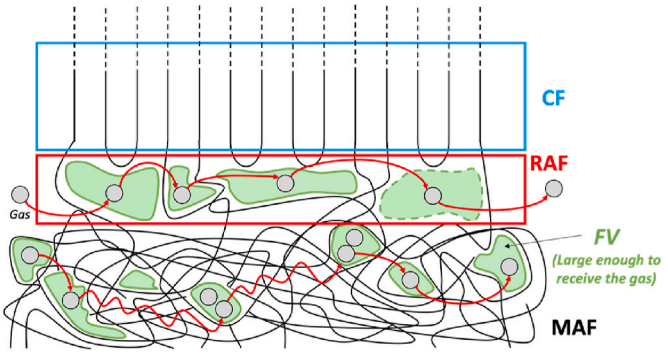

Fig. 18. Representation of the excess free volume in the rigid amorphous phase in PEKK inducing enhanced gas diffusion in the RAF and a slightly higher gas solubility in MAF.

configurations exists. While a concentration between 20 and 40%wt. has no effect on permeability in MAF (PEKK 6002 vs. PEKK 8002), higher concentrations in the zone surrounding the crystals significantly affect helium diffusion in RAF.

8. Conclusions

Comparison of PEKK grades with different T/I ratios and crystallinity rates enabled to study the impact of microstructure on permeability. Experimental results revealed that the T/I monomer ratio influences gas permeability of PEKK. The two-phase approach that is usually applied to model permeability of conventional polymers as a function of crystallinity failed here to explain the particular influence of the T/I ratio of PEKK grades. And in particular the fact 8002 PEKK grade is as permeable as 7002 and 6002 ones despite their different crystallinity rates. Tortuosity consideration for planar oriented crystallites gives fair permeability predictions with an overall error close to 10 %. But describing the PEKK microstructure using a three-phase Crystal/RAF/MAF approach improves understanding of the permeability results obtained, while providing clear trends concerning the influence of the T/I ratio. In particular, it appears that RAF plays a significant role in the diffusion and solubility of gas within these polymers, and in particular when increasing the degree of crystallinity. This could be linked to a change in RAF density as a function of PEKK grade induced by the exclusion of meta configurations of PEKK macromolecules from the crystals in the RAF.

However, these conclusions were drawn from the study of cold-crystallized PEKK films. The comparison with films crystallized from the melt then would allow analyzing the role of MAF and RAF with different crystalline microstructures. Moreover, although the results obtained in this study support the existence of distinct properties for the rigid and mobile amorphous fraction, tortuosity remains a pertinent approach and may influence gas permeation. An in-depth analysis of PEKK microstructure (orientation, crystallite sizes distribution, etc.) could provide useful information for considering the effect of tortuosity along with a three-phase model.

Finally, this study being a part of the HYPOCCRYT (Hydrogen Permeability of Organic Composites at Cryogenic Temperatures) project, polymers permeability will be investigated as a function of temperature, down to temperatures in the cryogenic range ($T < 120K$), i.e. as close as possible to the conditions under which LH2 tanks are used. The thermo-dependence of diffusion and solubility will be analyzed in detail, considering the role of RAF.

CRediT authorship contribution statement

T. Durand: Writing – original draft, Validation, Methodology, Investigation, Formal analysis, Data curation, Conceptualization. **O. De Almeida:** Writing – review & editing, Validation, Supervision, Resources, Project administration, Methodology, Investigation, Funding acquisition, Conceptualization.

Declaration of competing interest

The authors declare the following financial interests/personal relationships which may be considered as potential competing interests: Olivier De Almeida reports financial support was provided by Occitanie Region. If there are other authors, they declare that they have no known competing financial interests or personal relationships that could have appeared to influence the work reported in this paper.

Data availability

The authors do not have permission to share data.

Acknowledgments

We would like to express our warmest thanks to Dr. Quentin Sirvin for his outstanding contribution to the design and installation of the permeability test set-up. We also acknowledge the Occitanie Region, IMT Mines Albi and Airbus Operations SAS for funding the “Hydrogen Permeability of Organic Composites at Cryogenic Temperatures” (HYPOCCRYT) project. We would also like to thank Arkema for supplying the materials.

References

[1] N. Mazlan, S.M. Sapuan, et R.A. Ilyas, Advanced Composites in Aerospace Engineering Applications, Springer International Publishing, Cham, 2022, https://doi.org/10.1007/978-3-030-88192-4.

[2] Q. Cheng, R. Zhang, Z. Shi, et J. Lin, Review of common hydrogen storage tanks and current manufacturing methods for aluminium alloy tank liners, Int. J. Lightweight Mater. Manuf. (2023) S2588840423000434, https://doi.org/10.1016/j.ijlmm.2023.08.002 août.

[3] W. Gul, Y.E. Xia, P. Gérard, et S.K. Ha, Characterization of polymeric composites for hydrogen tank, Polymers 15 (18) (sept. 2023) 3716, https://doi.org/10.3390/polym15183716.

[4] P.K. Sandhya, R. Lakshmipriya, et M.S. Sreekala, « gas permeability through thermosets, in: Transport Properties of Polymeric Membranes, Elsevier, 2018, pp. 475–516, https://doi.org/10.1016/B978-0-12-809884-4.00023-9.

[5] J.E. Mark, Physical Properties of Polymers Handbook, second ed., Springer, New York, 2006.

[6] G. Eastmond, P. Page, J. Paprotny, R. Richards, , et al.R. Shaunak, Molecular weight dependence of gas permeability and selectivity in copolyimides, Polymer 34 (3) (1993) 667–670, https://doi.org/10.1016/0032-3861(93)90571-Q.

[7] F. Sarrasin, « Étude de la perméabilité de polymères semi-cristallins en présence de mélanges de gaz », p. 249.

[8] P. M. Namin, « Perméation des gaz dans les polymères semi-cristallins par modélisation moléculaire », p. 157.

[9] M.H. Klopffer, et B. Flaconneche, Transport properdines of gases in polymers: bibliographic review, Oil Gas Sci. Technol. Rev. IFP 56 (3) (2001) 223–244, https://doi.org/10.2516/ogst:2001021, mai.

[10] T. Choupin, « Mechanical Performances of PEKK Thermoplastic Composites Linked to Their Processing Parameters ».

[11] S. Füzesséry, Polyaryléthercétones PAEK, Plastiques et composites (1995), https://doi.org/10.51257/a-v1-a3395 févr.

[12] D.J. Blundell, et B.N. Osborn, The morphology of poly(aryl-ether-ether-ketone), Polymer 24 (8) (1983) 953–958, https://doi.org/10.1016/0032-3861(83)90144-1, août.

[13] D.J. Blundell, et A.B. Newton, Variations in the crystal lattice of PEEK and related para-substituted aromatic polymers: 2. Effect of sequence and proportion of ether and ketone links, Polymer 32 (2) (1991) 308–313, https://doi.org/10.1016/0032-3861(91)90019-F, janv.

[14] M.E. Pomatto, et R.B. Moore, Crystallization kinetics and equilibrium melting temperature of poly(ether ketone ketone) with high terephthalate content utilizing fast scanning calorimetry, Polymer 271 (2023) 125810, https://doi.org/10.1016/j.polymer.2023.125810 avr.

[15] K.H. Gardner, B.S. Hsiao, R.R. Matheson, et B.A. Wood, Structure, crystallization and morphology of poly (aryl ether ketone ketone), Polymer 33 (12) (1992) 2483–2495, https://doi.org/10.1016/0032-3861(92)91128-O, janv.

[16] S.Z.D. Cheng, R.-M. Ho, B.S. Hsiao, et K.H. Gardner, Polymorphism and crystal structure identification in poly(aryl ether ketone ketone)s, Macromol. Chem. Phys. 197 (1) (1996) 185–213, https://doi.org/10.1002/macp.1996.021970115, janv.

[17] L. Quiroga Cortés, N. Caussé, E. Dantras, A. Lonjon, et C. Lacabanne, Morphology and dynamical mechanical properties of poly ether ketone ketone (PEKK) with meta phenyl links, app, J. Appl. Polym. Sci. 133 (19) (2016) 43396, https://doi.org/10.1002/app.43396. mai.

[18] S.Z.D. Cheng, M.Y. Cao, et B. Wunderlich, « Glass transition and melting behavior of poly(oxy-1,4-phenyleneoxy-1,4-phenylenecarbonyl-1,4-phenylene) (PEEK), Macromolecules 19 (7) (1986) 1868–1876, https://doi.org/10.1021/ma00161a015, juill.

[19] M. Arous, I.B. Amor, A. Kallel, Z. Fakhfakh, et G. Perrier, Crystallinity and dielectric relaxations in semi-crystalline poly(ether ether ketone), J. Phys. Chem. Solid. 68 (7) (2007) 1405–1414, https://doi.org/10.1016/j.jpcs.2007.02.046, juill.

[20] J. Crank, The Mathematics of Diffusion, 2d ed., [Eng]: Clarendon Press, Oxford, 1975.

[21] C. Scholes, , et al.U. Ghosh, Review of membranes for helium separation and purification, Membranes 7 (1) (févr. 2017) 9, https://doi.org/10.3390/membranes7010009.

[22] R.K. Verma, V. Velikov, R.G. Kander, H. Marand, B. Chu, et B.S. Hsiao, SAXS studies of lamellar level morphological changes during crystallization and melting in PEEK, Polymer 37 (24) (nov. 1996) 5357–5365, https://doi.org/10.1016/S0032-3861(96)00387-4.

[23] M. Fatnassi, F.B.C. Larbi, A. Dubault, et J.L. Halary, Structural study of semi-crystalline blends of poly(vinylidene fluoride) and poly(methyl methacrylate) by means of linear correlation and interface distribution functions, E-Polymers 5 (1) (2005), https://doi.org/10.1515/epoly.2005.5.1.585 déc.

[24] S. Tencé-Girault, S. Lebreton, O. Bunau, P. Dang, et F. Bargain, Simultaneous SAXS-WAXS experiments on semi-crystalline polymers: example of PA11 and its brill transition, Crystals 9 (5) (2019) 271, https://doi.org/10.3390/cryst9050271, mai.
[25] B. R. Murray, C. M. Ó. Brádaigh, et S. B. Leen, « Characterisation of Rotationally Moulded Polymer Liners for Low Permeability Cryogenic Applications in Composite Overwrapped Pressure Vessels ».
[26] U. Sonchaeng, F. Iñiguez-Franco, R. Auras, S. Selke, M. Rubino, et L.-T. Lim, Poly (lactic acid) mass transfer properties, Prog. Polym. Sci. 86 (nov. 2018) 85–121, https://doi.org/10.1016/j.progpolymsci.2018.06.008.
[27] L. Monson, S.I. Moon, et C.W. Extrand, « Permeation resistance of poly(ether ether ketone) to hydrogen, nitrogen, and oxygen gases, J. Appl. Polym. Sci. 127 (3) (2013) 1637–1642, https://doi.org/10.1002/app.37517, févr.
[28] H. Kanesugi, K. Ohyama, H. Fujiwara, et S. Nishimura, High-pressure hydrogen permeability model for crystalline polymers, Int. J. Hydrogen Energy 48 (2) (2023) 723–739, https://doi.org/10.1016/j.ijhydene.2022.09.205, janv.
[29] K. Tanaka, H. Kita, K. Okamoto, A. Nakamura, et Y. Kusuki, The effect of morphology on gas permeability and permselectivity in polyimide based on 3,3′,4,4′-biphenyltetracarboxylic dianhydride and 4,4′-oxydianiline, Polym. J. 21 (2) (1989) 127–135, https://doi.org/10.1295/polymj.21.127, févr.
[30] L.E. Nielsen, Models for the permeability of filled polymer systems, J. Macromol. Sci. Part A - Chemistry 1 (5) (1967) 929–942, https://doi.org/10.1080/10601326708053745, août.
[31] R.K. Bharadwaj, Modeling the barrier properties of polymer-layered silicate nanocomposites, Macromolecules 34 (26) (2001) 9189–9192, https://doi.org/10.1021/ma010780b, déc.
[32] A. Leonardi, E. Dantras, J. Dandurand, et C. Lacabanne, Dielectric relaxations in PEEK by combined dynamic dielectric spectroscopy and thermally stimulated current, J. Therm. Anal. Calorim. 111 (1) (2013) 807–814, https://doi.org/10.1007/s10973-012-2548-3, janv.
[33] P. Huo, et P. Cebe, « Temperature-dependent relaxation of the crystal-amorphous interphase in poly(ether ether ketone), Macromolecules 25 (2) (1992) 902–909, https://doi.org/10.1021/ma00028a061, janv.
[34] L. Aliotta, M. Gazzano, A. Lazzeri, et M.C. Righetti, Constrained amorphous interphase in poly(l -lactic acid): estimation of the tensile elastic modulus, ACS Omega 5 (33) (2020) 20890–20902, https://doi.org/10.1021/acsomega.0c02330, août.
[35] R. Androsch, et B. Wunderlich, The link between rigid amorphous fraction and crystal perfection in cold-crystallized poly(ethylene terephthalate), Polymer 46 (26) (2005) 12556–12566, https://doi.org/10.1016/j.polymer.2005.10.099, déc.
[36] Y.S. Chun, Y.S. Han, J.C. Hyun, et W.N. Kim, Glass transition temperatures and rigid amorphous fraction of poly(ether ether ketone) and polyarylate blends, Polymer 41 (24) (nov. 2000) 8717–8720, https://doi.org/10.1016/S0032-3861(00)00301-3.
[37] B. Wunderlich, The ATHAS database on heat capacities of polymers, Pure Appl. Chem. 67 (6) (1995) 1019–1026, https://doi.org/10.1351/pac199567061019, janv.
[38] Heon Sang Lee, et Woo Nyon Kim, Glass transition temperatures and rigid amorphous fraction of poly(ether ether ketone) and poly(ether imide) blends, Polymer 38 (11) (1997) 2657–2663, https://doi.org/10.1016/S0032-3861(97)85599-1, mai.
[39] V.P. Swapna, V.S. Abhisha, et R. Stephen, Polymer/polyhedral oligomeric silsesquioxane nanocomposite membranes for pervaporation, in: Polymer Nanocomposite Membranes for Pervaporation, Elsevier, 2020, pp. 201–229, https://doi.org/10.1016/B978-0-12-816785-4.00009-4.
[40] S. Marano, E. Laudadio, C. Minnelli, et P. Stipa, Tailoring the barrier properties of pla: a state-of-the-art review for food packaging applications, Polymers 14 (8) (avr. 2022) 1626, https://doi.org/10.3390/polym14081626.
[41] A. Guinault, C. Sollogoub, V. Ducruet, et S. Domenek, Impact of crystallinity of poly(lactide) on helium and oxygen barrier properties, Eur. Polym. J. 48 (4) (2012) 779–788, https://doi.org/10.1016/j.eurpolymj.2012.01.014, avr.
[42] M.A. Islam, et H. Buschatz, Gas permeation through a glassy polymer membrane: chemical potential gradient or dual mobility mode? Chem. Eng. Sci. 57 (11) (2002) 2089–2099, https://doi.org/10.1016/S0009-2509(02)00068-4, juin.
[43] P. Li, T.S. Chung, et D.R. Paul, Gas sorption and permeation in PIM-1, J. Membr. Sci. 432 (2013) 50–57, https://doi.org/10.1016/j.memsci.2013.01.009, avr.
[44] A.S. Michaels, et H.J. Bixler, Solubility of gases in polyethylene, J. Polym. Sci. 50 (154) (1961) 393–412, https://doi.org/10.1002/pol.1961.1205015411, avr.
[45] P. Tremblay, M. Savard, J. Vermette, et R. Paquin, Gas permeability, diffusivity and solubility of nitrogen, helium, methane, carbon dioxide and formaldehyde in dense polymeric membranes using a new on-line permeation apparatus, J. Membr. Sci. 282 (1–2) (oct. 2006) 245–256, https://doi.org/10.1016/j.memsci.2006.05.030.
[46] B.J. Briscoe, et H. Mahgerefteh, Absorption of nitrogen and helium in poly (tetrafluoroethylene), Philos. Mag. A 53 (5) (1986) 645–651, https://doi.org/10.1080/01418618608242862, mai.
[47] A.S. Michaels, H.J. Bixler, et H.L. Fein, Gas transport in thermally conditioned linear polyethylene, J. Appl. Phys. 35 (11) (nov. 1964) 3165–3178, https://doi.org/10.1063/1.1713195.